The effect of shear rate on aggregate size distribution and structure at steady state: a comparison between a Taylor–Couette reactor and a mixing tank

P. Bubakova, M. Pivokonsky, R. Pivokonsky and P. Filip

ABSTRACT

The paper deals with the dependence of aggregate properties on the shear rate (G) at steady state. Aggregation of natural raw water and ferric sulphate was carried out in a laboratory Taylor–Couette reactor (TC) and continuous flow mixing tank (MT) with a paddle stirrer. Shear rates in the range of 20–350 s^{-1} were used. Methods of image and fractal analyses were used to determine the aggregate size and structure, respectively. It was found that the aggregate size decreased with increasing shear rate. There was a small difference in sizes of aggregates formed in TC and MT at $G < 150\ s^{-1}$, but at higher shear rates, almost no difference between TC and MT was observed. The D_2 fractal dimension increased with increasing shear rate indicating that aggregates became less porous and more compact. Moreover, a very close match in D_2 values was attained for both mixing devices. The D_{pf} fractal dimension decreased with increasing shear rate meaning that aggregates were more regular at higher shear rates, but jagged on the surface with irregular shape at lower shear rates. In contrast to D_2, aggregates formed in MT were much more irregular (jagged) than those formed in TC.

Key words | aggregate size distribution, aggregation, flocculation, fractal dimension, shear rate

P. Bubakova
M. Pivokonsky (corresponding author)
R. Pivokonsky
P. Filip
Institute of Hydrodynamics,
Academy of Sciences of the Czech Republic,
Pod Patankou 5,
16612 Prague 6,
Czech Republic
E-mail: *pivo@ih.cas.cz*

LIST OF SYMBOLS

A	projected area of aggregate [m^2]
B	adjustable parameter [m]
C	aggregate strength constant in Equation (4) [–]
d	aggregate diameter/size [m]
d_0	primary particle size [m]
D_2	2D cluster fractal dimension [–]
d_{avr}	average aggregate diameter [m]
d_{mp}	most probable aggregate diameter [m]
D_{pf}	2D perimeter-based fractal dimension [–]
f	rotation frequency [s^{-1}]
G	global velocity gradient [s^{-1}]
H	height of Taylor–Couette reactor [m]
k	proportional coefficient in Equation (5) [s^m]
m	power law coefficient in Equation (5) [–]
M	torque [$kg\ m^2\ s^{-2}$]
P	aggregate perimeter [m]
P_i	power dissipated in the aggregation space [$kg\ m^2\ s^{-3}$]
R	Reynolds number ratio (Re/Re_c) [–]
R_1	inner radius of Taylor–Couette reactor [m]
R^2	index of determination [–]
R_2	outer radius of Taylor–Couette reactor [m]
Re	Reynolds number [–]
Re_c	critical Reynolds number [–]
T	time of aggregation in Taylor–Couette reactor [s]
V	volume of aggregation space in Taylor–Couette reactor [m^3]
w	gap width in Taylor–Couette reactor ($R_2 - R_1$) [m]
γ	aggregate strength constant in Equation (4) [–]
Γ	aspect ratio of Taylor–Couette reactor (H/w) [–]
ε	energy dissipation rate [$m^2\ s^{-3}$]
η	radius ratio of Taylor–Couette reactor (R_1/R_2) [–]
μ	dynamic viscosity of fluid [$kg\ m^{-1}\ s^{-1}$]
ω	angular velocity of inner cylinder rotation [$rad\ s^{-1}$]

doi: 10.2166/aqua.2013.005

INTRODUCTION

The processes of destabilisation and aggregation are traditionally used to remove colloidal particles in water treatment. The purpose is to prepare aggregates of such properties (size, structure, shape, density, etc.) that are suitable for reaching the maximum effectiveness of following separation steps, such as sedimentation, filtration or flotation. During the aggregation process, the particles collide with each other and form bigger aggregates. However, as the aggregates grow, they become susceptible to break-up by fluid shear. After a certain time, the aggregate properties reach a steady state between aggregate growth and break-up and they do not change any more (Spicer *et al*. 1996).

The properties of formed aggregates depend on the balance between the hydrodynamic and cohesive force. The hydrodynamic force arises from a flow of fluid around a particle and is thus determined by the magnitude and distribution of the shear rate (G), cross-sectional area of a primary particle and dynamic viscosity of fluid. The cohesive force is given by the sum of all attractive forces acting between interacting particles (e.g., van der Waals, electrostatic or hydrophobic forces). It depends particularly on the particle (and/or reagent) composition; number concentration and size of primary particles; and the arrangement of primary particles in an aggregate (Tambo & Hozumi 1979; Francois 1987; Spicer & Pratsinis 1996; Jarvis *et al*. 2005).

The aim of this paper is to describe the influence of the global shear rate on the steady state properties of aggregates formed in the aggregation process; and, furthermore, to compare the aggregation in two different mixing devices: a Taylor–Couette (TC) reactor (laboratory batch test) and mixing tank (MT) with a paddle stirrer (continuous pilot plant).

METHODS

Raw water and reaction conditions

The experiment used raw water from the Svihov reservoir (potable water source), Czech Republic. The tests were carried out during the winter period (January) when raw water quality was stable with the parameters given in Table 1.

Table 1 | Quality of raw water

Parameter	Value	Parameter	Value
T [°C]	3.6	TOC [mg L^{-1}]	4.4
pH [–]	7.2	DOC [mg L^{-1}]	3.8
Alkalinity [mmol L^{-1}]	1.09	Fe [mg L^{-1}]	0.05
Turbidity [NTU]	2.9	TSS [mg L^{-1}]	22.6

TOC, total organic carbon; DOC, dissolved organic carbon; TSS, total suspended solids.

Another advantage of winter water is that the content of suspended solids and organic matter is relatively low. Ferric sulphate hydrate $Fe_2(SO_4)_3 \cdot 9H_2O$ (Analytika Ltd, Czech Republic) served as coagulant. Its dose (3.98 mg L^{-1} of Fe) was optimised by standard jar tests.

Mixing conditions

The experiments were carried out in two types of mixing device: a TC reactor (laboratory batch device) and a MT with the paddle stirrer (continuous/flow-through pilot plant). All experiments were carried out at a temperature of 3.6 °C.

Taylor–Couette reactor

The TC reactor consisted of a pair of concentric cylinders, with an inner rotating cylinder. The inner cylinder had a radius of $R_1 = 76$ mm and the outer a radius of $R_2 = 85.5$ mm, which results in a gap width of $w = R_2 - R_1 = 9.5$ mm and radius ratio of $\eta = R_1/R_2 = 76/85.5 = 0.889$. The height of the cylinders was $H = 350$ mm resulting in the aspect ratio of $\Gamma = H/w = 350/9.5 = 36.8$. Both cylinders were made of Plexiglas (Umaplex, Perspex); the inner one was painted white, and served as a contrast background for the aggregates having an orange-brownish colour. The outer cylinder was transparent and allowed the photographic imaging of the aggregation process. The inner cylinder was driven by a variable speed drive with a torque-meter. The hydrodynamic conditions in TC were characterised by the global shear rate G calculated according to the relationship as follows (Camp & Stein 1943):

$$G = \sqrt{\frac{P_i}{V\mu}} = \sqrt{\frac{\omega M}{V\mu}} = \sqrt{\frac{2\pi f M}{V\mu}}, \quad (1)$$

where P_i represents the power dissipated in the aggregation space, V is the volume of the aggregation space, μ is the dynamic viscosity of the fluid, ω is the angular velocity of inner cylinder rotation, M is the torque and f is the rotation frequency. The global shear rates used in TC were $G = 21.2$, 38.7, 58.9, 79.8, 102.3, 149.1, 202.2, 252.8, 300.5 and 347.9 s^{-1}. The retention period of the suspension in the TC corresponded to $T = 15$ min, which was the time when the steady state was reached. The flow regime in TC can be characterised by the means of Reynolds number ratio $R = Re/Re_c$, where Re_c is the critical Reynolds number depending upon the specific geometry (i.e., the radius and aspect ratio) of the TC used (DiPrima *et al.* 1984; Wang *et al.* 2005). It follows from the literature that the flow regime in TC varied in dependence on the used global shear rates from wavy vortex flow to turbulent vortex flow, transition at $R \sim 35$ (G between 40 and 60 s^{-1}) and, further, to fully developed turbulence, $R > 100$ (G between 150 and 200 s^{-1}) (Takeda 1999; Wang *et al.* 2005).

Mixing tank – pilot plant

The pilot plant consisted of a dosing unit and MT. Dosed raw water flowed into the MT made of a Plexiglas tube. The geometry of the MT is illustrated in Figure 1. The stirrer had four paddles connected with five transverse crosspieces and it was driven by a variable speed drive with a torque-meter. The spot/location of photographic imaging of aggregates is marked as CTI (centre of taken images) in Figure 1. The hydrodynamic conditions in the MT were characterised by the global shear rate G calculated by Equation (1). The global shear rates used in the MT were $G = 28.4$, 45.2, 77.4, 114.1, 153.2, 199.2, 244.1 and 307.2 s^{-1}.

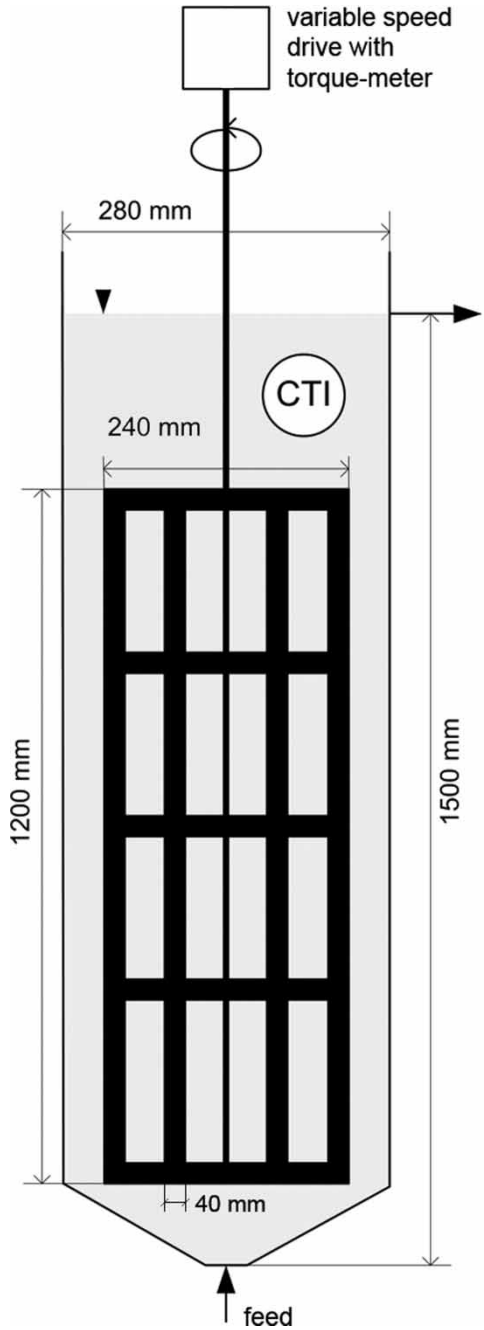

Figure 1 | Mixing tank design.

Analyses of aggregate properties

Image analysis

The size of aggregates formed during the aggregation process in the TC and MT was determined by image analysis. It was based on three steps:

1. Illuminating a slice of flow in the aggregation reactor with a laser light sheet (width = 1.2 ± 0.1 mm) generated by a laser diode ($\lambda = 675$ nm, power capacity 20 mW).
2. Recording images of the aggregate using a digital camera Pentax K20D (Asahi Co., Japan) with a Sigma AF 105/2.8 EX MACRO lens – magnification 1:1 (Sigma Co., Japan).
3. Processing the images using image analysis software (Sigma Scan 5).

The digital images (22 × 14.6 mm) were taken in RAW format (4,672 × 3,104 pixels), which resulted in a pixel size of about 4.7 × 4.7 μm. In order to eliminate the digital background noise, only aggregates larger than 4 pixels (9.4 × 9.4 μm) were retained in the image analysis process. The images were then converted from RAW format to BMP grey-scale format and the Sigma Scan 5 software was used to calculate the projected area A and perimeter P of all imaged aggregates. The equivalent aggregate diameter d [μm] of each aggregate was calculated from the projected area. Furthermore, the average aggregate diameter d_{avr} and most probable aggregate diameter d_{mp} were calculated. This image processing technique is described in detail in the literature (Pivokonsky *et al.* 2003; Bouyer *et al.* 2004; Bubakova & Pivokonsky 2012).

Fractal analysis

A two-dimensional cluster fractal dimension D_2 was used to characterise the aggregate structure. It was calculated by the following equation from the slope of the log-log plot of the equivalent aggregate diameter d vs. the projected area of the aggregate A (Jiang & Logan 1991; Gorczyca & Ganczarczyk 1999; Chakraborti *et al.* 2007; Xiao *et al.* 2009):

$$A \propto d^{D_2}. \quad (2)$$

Densely packed (i.e., less porous) aggregates have a high fractal dimension, while a lower fractal dimension results from large, highly branched and loosely bound structures (Jiang & Logan 1996; Haarhoff & Edzwald 2004; Rahmani *et al.* 2005; Li *et al.* 2006; Chakraborti *et al.* 2007; Bache & Gregory 2010).

The geometry (or shape, regularity, surface morphology) of aggregates was evaluated with the use of the perimeter-based fractal dimension D_{pf} defined by the relationship between the measured perimeter P and the projected area A of the aggregate (Spicer *et al.* 1996; Meakin 1998; Rahmani *et al.* 2005; Soos *et al.* 2007, 2008):

$$A \propto P^{2/D_{pf}}, \quad (3)$$

where D_{pf} is the perimeter-based fractal dimension of the aggregate. The values of D_{pf} were obtained (similarly as in the case of D_2) from the slope of the log-log plot of aggregate perimeter vs. projected area. They vary between 1 (regular, circular shape) and 2 (irregular, jagged surface, non-circular shape). The interpretation of increasing D_{pf} is as follows: as the projected area (A) of the fractal aggregate increases, the aggregate perimeter (P) increases more rapidly than for Euclidean objects, so that the boundary becomes more convoluted (Spicer *et al.* 1996; Rahmani *et al.* 2005).

RESULTS AND DISCUSSION

The suspension formed in two different mixing devices – a TC reactor (laboratory scale, batch test) and a MT with a paddle stirrer (pilot plant scale, continuous measurement) – was characterised from the point of view of its properties in dependence on the shear rate.

Aggregate/particle size distribution (PSD) – most probable, average and maximum diameter

PSD

The size distributions of aggregates formed in TC and MT are plotted in Figures 2(a) and 2(b). It is apparent that they are very similar to each other. Generally, it can be concluded that the aggregate size distribution is narrower with increasing G value. The suspension with heterogeneous aggregate size distribution homogenises due to increasing hydrodynamic force. At low G values, considerably large aggregates form; nevertheless, smaller aggregates occur simultaneously in the system. An example is demonstrated at the shear rates $G = 21.2\ s^{-1}$ (TC) and $28.4\ s^{-1}$ (MT) with the greatest variability in formed aggregates, where aggregates from 9.4 up to 7,806 and 6,918 μm are present in the TC and MT, respectively. In contrast, the lowest variability in formed aggregates occurs at global shear rates $G = 347.9\ s^{-1}$ (TC) and $307.2\ s^{-1}$ (MT) where only aggregates from 9.4 to 235 and 249 μm, respectively, are present. Furthermore, the aggregate size distribution is practically identical at shear rates $G \geq 200\ s^{-1}$ for aggregates formed in TC as well as MT. At such conditions, the influence of hydrodynamic force on aggregate size is almost indistinguishable.

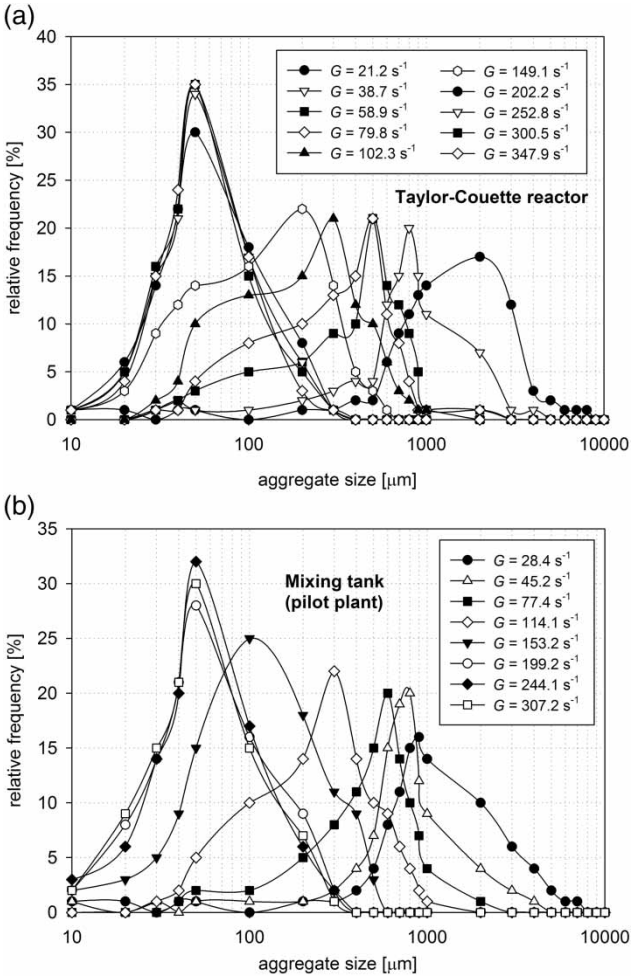

Figure 2 | Size distribution of aggregates formed in (a) the Taylor–Couette reactor and (b) the mixing tank.

Most probable aggregate diameter

From the aggregate size distribution (Figures 2(a) and 2(b)), a characteristic aggregate scale can be defined: the most probable aggregate diameter d_{mp} (Bouyer *et al.* 2004) which has the highest representation in the size distribution (it is the diameter that corresponds to the top of the peak of the size distribution curve). The most probable aggregate diameter, which varies from 50 to 2,000 μm in TC and from 50 to 900 μm in MT, decreases with increasing G. If $G > 150\ s^{-1}$, the peak representing the most probable aggregate diameter is much more distinct than at shear rates lower than $150\ s^{-1}$. Figure 2(a) shows that whereas at $G = 21.2\ s^{-1}$, the most probable aggregate diameter represents approximately 17% of the total number of aggregates, at $G > 250\ s^{-1}$ (approximately), it is twice as much (35%). Similar results were obtained in the case of MT as well.

Average/maximum aggregate diameter

Many authors have studied the relationship between the aggregate size and shear rate using the following empirical expression (Argaman & Kaufman 1970; Tambo & Hozumi 1979; Francois 1987; Mühle 1993; Bache *et al.* 1999; Bouyer *et al.* 2004; Coufort *et al.* 2005; Serra *et al.* 2008; Bubakova & Pivokonsky 2012):

$$d_{avr/max} = C\varepsilon^{-\gamma} = CG^{-2\gamma} \quad (4)$$

where ε is the energy dissipation rate; and C and γ are aggregate strength constants for given system and conditions comprising parameters such as the type and magnitude of interactions, size and number of primary particles, etc., and possibly the density and viscosity of water or suspension (Mühle 1993). The mentioned expression is a decreasing power function fitted to the measured data at an intermediate shear rate (Francois 1987; Mühle 1993; Bache *et al.* 1999; Bouyer *et al.* 2004; Serra *et al.* 2008; Bubakova & Pivokonsky 2012). The functional form of Equation (4) supposes symmetrical behaviour with respect to both axes, i.e., a uniform approach both to the abscissa (shear rate) and to the ordinate (average/maximum aggregate diameter). Nevertheless, more detailed analysis of the experimental data shows a certain degree of asymmetry. This can be respected by the following equation:

$$d_{avr/max} = \frac{B}{1 + kG^m}, \quad (5)$$

where B is the adjustable parameter, k is the proportional coefficient and m is the power law coefficient.

The result of fitting the proposed model (Equation (5)) to the measured data is presented in Figures 3(a) and 3(b). Owing to the discussion in the literature about whether the maximum or average aggregate size should occur in the relationship (Jarvis *et al.* 2005), both values were determined. Figures 3(a) and 3(b) show that the proposed model (Equation (5)) describes the measured data very well with indices of determination $R^2 = 0.998$ for TC and 0.993 for MT in the

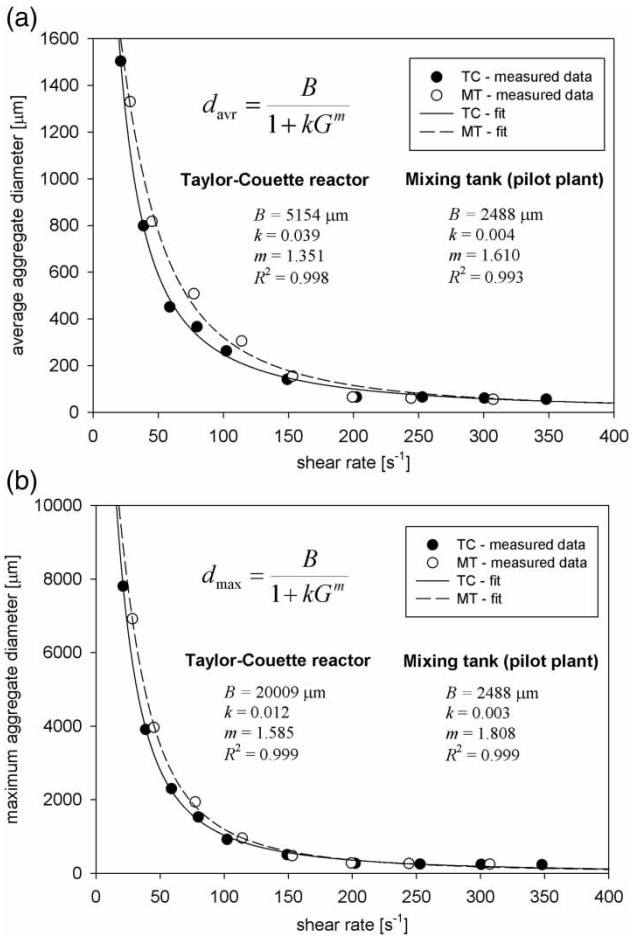

Figure 3 | (a) Fitting the proposed model to the measured data – the dependence of average aggregate diameter on the shear rate at steady state. (b) Fitting the proposed model to the measured data – the dependence of maximum aggregate diameter on the shear rate at steady state.

case of average aggregate diameter; and $R^2 = 0.999$ for both TC and MT in the case of maximum aggregate diameter.

When the steady state size of aggregates formed in TC and MT is compared, it can be seen that the maximum size of aggregates produced by both mixing devices is very similar (Figure 3(b)). Nevertheless, there is a little difference in the average aggregate size. According to the fitted model, the average aggregate size in MT is higher than in the TC device at $G = 40$–$150\ s^{-1}$. The highest difference in the measured data can be seen at $G \sim 80\ s^{-1}$ (Figure 3(a)). To better understand this phenomenon, the aggregate size distribution of aggregates formed at $G \sim 80\ s^{-1}$ was plotted on a graph in Figure 4. For comparison, the same data for $G \sim 150\ s^{-1}$ (where there is almost no difference in average aggregate size) were added. Figure 4 shows that the difference

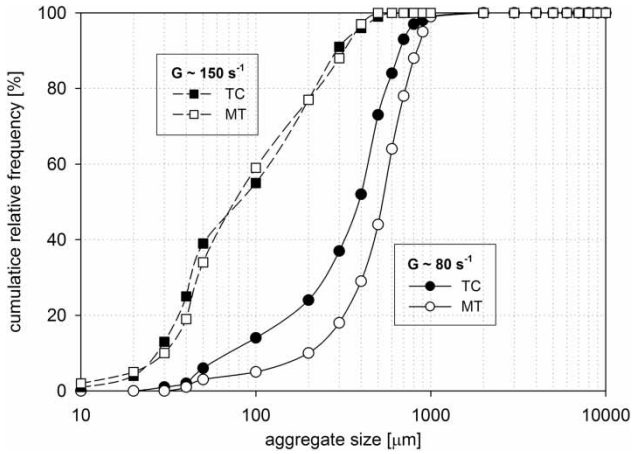

Figure 4 | Aggregate size distributions in the Taylor–Couette reactor and the mixing tank at $G \sim 80$ and $150\ s^{-1}$.

between the size of aggregates formed in TC and MT at $G \sim 80\ s^{-1}$ is caused by the phase shift of PSD cumulative curves. In other words, there is a bigger amount of smaller aggregates ($\leq$500 μm) and simultaneously, a lesser amount of larger aggregates ($\geq$600 μm) in TC than in MT.

Fractal dimension

It is well known that aggregates are typical fractal objects (Meakin 1998) and fractal analysis has become to be used for characterising the aggregate structure. In this paper, two-dimensional data were gained from the image analysis and, therefore, only the D_2 and D_{pf} fractal dimensions could be calculated.

The D_2 fractal dimension is considered to reflect the aggregate compactness (Jiang & Logan 1996). The higher the D_2, the more compact aggregates are. For applied shear rates, the D_2 fractal dimension was found to range from 1.54 to 1.91 in TC and from 1.58 to 1.90 in MT (Figure 5(a)). It became higher with increasing shear rate, indicating that the aggregates became less porous and more compact (Gorczyca & Ganczarczyk 1999; Rahmani *et al.* 2005; Chakraborti *et al.* 2007). Moreover, a very close match in D_2 values was attained for both mixing devices.

The D_{pf} fractal dimension generally represents the shape (or regularity) of an aggregate. The more it approaches the value of 1, the more regular the aggregates are. Our measurements showed that D_{pf} decreased from 1.37 to 1.10 in TC and from 1.36 to 1.12 in MT with increasing G value (Figure 5(b)).

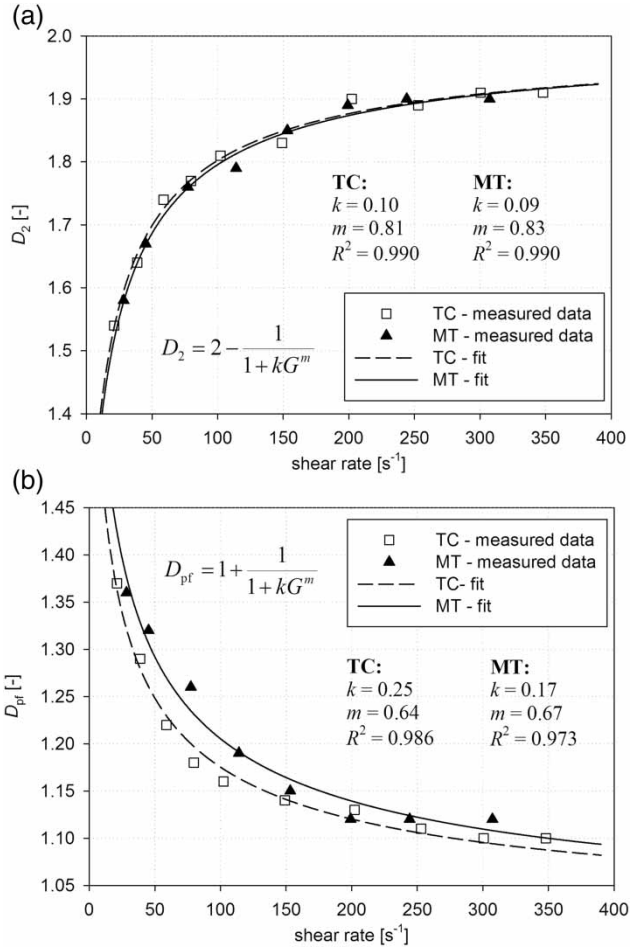

Figure 5 | The dependence of fractal dimensions on the shear rate at steady state for the Taylor–Couette reactor and the mixing tank; (a) D_2 fractal dimension, (b) D_{pf} fractal dimension.

At higher shear rates, the D_{pf} values were lower, which indicates more regular aggregates. In contrast, at the low shear rates, the D_{pf} values were higher, which means the aggregates are more jagged on the surface with an irregular shape. In contrast to the D_2 fractal dimension, there is a significant difference in D_{pf} values of aggregates formed in TC and MT. It follows from Figure 5(b) that aggregates formed in MT are much more irregular or jagged than those formed in TC. This difference is undoubtedly the result of different flow regimes in the mixing devices used. Nevertheless, considering that only D_{pf} changes for TC and MT and D_2 remain identical, it suggests itself that non-uniformities of local shear rates in MT cause aggregates to be eroded on the surface and the inner structure is not influenced by the flow regime to such an extent.

The functional dependence of G in Equation (5) was also used for a description of the fractal dimensions D_2 and D_{pf} in dependence on shear rate. With respect to the definitions of D_2 and D_{pf}, the parameter B was set to $B = 1$. The fits for D_2 presented in Figure 5(a) give a very good result with $R^2 = 0.990$ for TC and $R^2 = 0.990$ for MT. In the case of D_{pf} (Figure 5(b)), the result of fitting the proposed model was less accurate, but still with the values of $R^2 = 0.986$ for TC and $R^2 = 0.973$ for MT.

CONCLUSIONS

- The aggregate size distribution was narrower with increasing shear rate. The suspension with heterogeneous aggregate size distribution homogenised due to increasing hydrodynamic force. Furthermore, the aggregate size distribution was practically identical at shear rates $G \geq 200\ s^{-1}$ for aggregates formed in TC as well as MT.
- The maximum steady state size of aggregates produced by both mixing devices was almost identical and ranged approximately from 7,800 μm at $G \sim 20\ s^{-1}$ to 245 μm at $G \sim 300\ s^{-1}$. In the case of the average aggregate size, there was a little difference at $G \sim 80\ s^{-1}$ when the aggregate size in the MT was higher than in the TC device.
- The extension of the relationship $d_{avr/max} = CG^{-2\gamma}$ which describes the dependence of aggregate diameter on the shear rate was proposed: $d_{avr/max} = B/(1 + kG^m)$. It takes into consideration an 'asymmetry' of aggregate size behaviour.
- With respect to the definitions of the fractal dimensionless D_2 and D_{pf}, the relations $D_{avr/max}$ vs. G and D_2/D_{pf} vs. G should be coupled to some extent. This is reflected in the possibility of applying the functional dependence of G proposed in Equation (5) to both cases.
- For applied shear rates, the D_2 fractal dimension was found to range from 1.54 to 1.91 in the TC and from 1.58 to 1.90 in the MT. It became higher with increasing shear rate indicating that the aggregates became less porous and more compact. Moreover, a very close match in D_2 values was attained for both mixing devices.
- With increasing shear rate, the D_{pf} fractal dimension decreased from 1.37 to 1.10 in the TC and from 1.36 to 1.12 in the MT. It means that aggregates are more regular at higher shear rates, but jagged on the surface with

irregular shapes at lower shear rates. In contrast to D_2, a difference between D_{pf} of aggregates formed in the TC and MT was observed: aggregates formed in the MT were much more irregular or jagged than those formed in TC.

- It follows from the presented results that it is possible to attain very similar results of aggregation in the continuous pilot plant as in the laboratory batch tests, if the stirrer geometry is well designed.

ACKNOWLEDGEMENTS

This research project was funded by the Czech Science Foundation under project No. P105/11/0247. The authors acknowledge financial assistance on this project.

REFERENCES

Argaman, Y. & Kaufman, W. J. 1970 Turbulence and flocculation. *J. Sanit. Eng. Div.* **96** (2), 223–241.

Bache, D. H. & Gregory, R. 2010 Flocs and separation processes in drinking water treatment: a review. *J. Water SRT – AQUA* **59** (1), 16–30.

Bache, D. H., Rasool, E. R., Moffat, D. & McGilligan, F. J. 1999 On the strength and character of alumino-humic flocs. *Water Sci. Technol.* **40** (9), 81–88.

Bouyer, D., Liné, A. & Do-Quang, Z. 2004 Experimental analysis of floc size distribution under different hydrodynamics in a mixing tank. *AIChE J.* **50** (9), 2064–2081.

Bubakova, P. & Pivokonsky, M. 2012 Influence of velocity gradient on properties and filterability of suspension formed during water treatment. *Sep. Purif. Technol.* **92**, 161–167.

Camp, T. R. & Stein, P. C. 1943 Velocity gradient and internal work in fluid motion. *J. Boston Soc. Civil Eng.* **30**, 219–237.

Chakraborti, R. K., Garner, K. H., Kaur, J. & Atkinson, F. J. 2007 *In situ* analysis of flocs. *J. Water SRT – AQUA* **56** (1), 1–11.

Coufort, C., Bouyer, D. & Line, A. 2005 Flocculation related to local hydrodynamics in Taylor–Couette reactor and in a jar. *Chem. Eng. Sci.* **60** (8–9), 2179–2192.

DiPrima, R. C., Eagles, P. M. & Ng, B. S. 1984 The effect of radius ratio on the stability of Couette flow and Taylor vortex flow. *Phys. Fluids* **27** (10), 2403–2411.

Francois, R. J. 1987 Strength of aluminium hydroxide flocs. *Water Res.* **21** (9), 1023–1030.

Gorczyca, B. & Ganczarczyk, J. 1999 Structure and porosity of alum coagulation flocs. *Water Qual. Res. J. Can.* **34** (4), 653–666.

Haarhoff, J. & Edzwald, J. K. 2004 Dissolved air flotation modelling: insights and shortcomings. *J. Water SRT – AQUA* **53** (3), 127–150.

Jarvis, P., Jefferson, B., Gregory, J. & Parsons, S. A. 2005 A review of floc strength and breakage. *Water Res.* **39** (14), 3121–3137.

Jiang, Q. & Logan, B. E. 1991 Fractal dimensions of aggregates determined from steady state size distributions. *Environ. Sci. Technol.* **36** (4), 2031–2038.

Jiang, Q. & Logan, B. E. 1996 Fractal dimensions of aggregates produced in laminar and turbulent shear devices. *J. AWWA* **88** (2), 100–113.

Li, T., Zhu, Z., Wang, D., Yao, Ch. & Tang, H. 2006 Characterization of floc size, strength and structure under various coagulation mechanisms. *Powder Technol.* **168** (2), 104–110.

Meakin, P. 1998 *Fractals, Scaling and Growth far from Equilibrium*. Cambridge University Press, New York.

Mühle, K. 1993 Floc stability in laminar and turbulent flow. In: *Coagulation and Flocculation* (B. Dobias, ed.). Marcel Dekker, New York, pp. 355–390.

Pivokonsky, M., Pivokonsky, R., Benesova, L. & Mutl, S. 2003 Methodology of evaluation of size and size-distribution of particles formed during aggregation. *J. Hydrol. Hydromech.* **51** (4), 281–287.

Rahmani, N. H. G., Dabros, T. & Masliyah, J. H. 2005 Fractal structure of asphaltene aggregates. *J. Colloid Interface Sci.* **285** (2), 599–608.

Serra, T., Colomer, J. & Logan, B. E. 2008 Efficiency of different shear devices on flocculation. *Water Res.* **42** (4–5), 1113–1121.

Soos, M., Wang, L., Fox, R. O., Sefcik, J. & Morbidelli, M. 2007 Population balance modeling of aggregation and breakage in turbulent Taylor–Couette flow. *J. Colloid Interface Sci.* **307** (2), 433–446.

Soos, M., Moussa, A. S., Ehrl, L., Sefcik, J., Wu, H. & Morbidelli, M. 2008 Effect of shear rate on aggregate size and morphology investigated under turbulent conditions in stirred tank. *J. Colloid Interface Sci.* **319** (2), 577–589.

Spicer, P. T. & Pratsinis, S. E. 1996 Shear-induced flocculation: the evolution of floc structure and the shape of the size distribution at steady state. *Water Res.* **30** (5), 1049–1056.

Spicer, P. T., Keller, W. & Pratsinis, S. E. 1996 The effect of impeller type on floc size and structure during shear-induced flocculation. *J. Colloid Interface Sci.* **184** (1), 112–122.

Takeda, Y. 1999 Quasi-periodic state and transition to turbulence in a rotating Couette system. *J. Fluid Mech.* **389** (1), 81–99.

Tambo, N. & Hozumi, H. 1979 Physical characteristics of flocs – II. Strength of floc. *Water Res.* **13** (5), 421–427.

Wang, L., Olsen, M. G. & Vigil, R. D. 2005 Reappearance of azimuthal waves in turbulent Taylor–Couette flow at large aspect ratio. *Chem. Eng. Sci.* **60** (20), 5555–5568.

Xiao, F., Zhang, B., Ma, J., Yi, P. & Cui, Ch. 2009 Effects of low temperature on floc fractal dimensions and shape factors during alum coagulation. *J. Water SRT – AQUA* **58** (1), 21–27.

First received 13 December 2012; accepted in revised form 7 May 2013